EEET ECOLOGICAL ENGINEERING & ENVIRONMENTAL TECHNOLOGY

Ecological Engineering & Environmental Technology, 2026, 27(8), 61–73
https://doi.org/10.12912/27197050/224814
ISSN 2719–7050, License CC-BY 4.0

Received: 2026.06.05
Accepted: 2026.07.10
Published: 2026.08.01

Dual role of zinc oxide nanoparticles in *Chromochloris zofingiensis*: Concentration-dependent toxicity and enhanced astaxanthin production

Erna Kristianti[1], Nasrullah Bai Arifin[2,3], Ating Yuniarti[2,3], Muhammad Fakhri[2,3*]

[1] Master Program of Aquaculture, Faculty of Fisheries and Marine Science, Universitas Brawijaya, Malang 65145, East Java, Indonesia
[2] Study Program of Aquaculture, Faculty of Fisheries and Marine Science, Universitas Brawijaya, Malang 65145, East Java, Indonesia
[3] Aquatic Biofloc Research Group, Universitas Brawijaya, Malang 65145, East Java, Indonesia
* Corresponding author's e-mail: mfakhri@ub.ac.id

ABSTRACT

Chromochloris zofingiensis is a promising microalga for producing high-value metabolites, particularly astaxanthin and lipids. This study evaluated the concentration-dependent effects of zinc oxide nanoparticles on growth, biomass production, photosynthetic pigments, astaxanthin, protein, and lipid accumulation in *C. zofingiensis*. The commercial ZnO-NPs, characterized before biological application, exhibited crystalline wurtzite structures with nanosized primary particles of approximately 50–100 nm that formed larger agglomerates. The microalga was cultivated in a standard BG-11 control medium containing zinc sulfate heptahydrate (0.22 mg L^{-1}) and in zinc-free BG-11 medium supplemented with ZnO-NPs at concentrations of 0, 0.06, 6, 30, and 60 mg L^{-1}. Physiological and biochemical responses were assessed through growth analysis, biomass measurement, pigment and astaxanthin determination, and proximate biochemical analysis. ZnO-NPs markedly altered microalgal metabolism in a dose-dependent manner. Growth and biomass were relatively maintained at low to moderate concentrations but declined under higher exposure levels. Chlorophyll a+b showed strong sensitivity to ZnO-NPs, with substantial reductions at 6–60 mg L^{-1}, while total carotenoids were comparatively more retained. Interestingly, the highest astaxanthin concentration was obtained at 6 mg L^{-1}, indicating that moderate ZnO-NP exposure induced a protective secondary carotenoid response. Protein content increased with mild exposure, whereas lipid content decreased at 6 mg L^{-1}, suggesting a redistribution of carbon flux toward stress-defense metabolism rather than storage lipid accumulation. These findings reveal a physiological boundary between ZnO-NP toxicity and nano-biostimulation in C. zofingiensis. Controlled exposure to ZnO-NPs may therefore provide a promising strategy for enhancing astaxanthin production in microalgal biotechnology.

Keywords: *Chromochloris zofingiensis*, zinc oxide nanoparticles, nano-biostimulation, astaxanthin production, toxicity.

INTRODUCTION

Microalgae are increasingly recognized as promising biological platforms for producing high-value metabolites, including proteins, lipids, polyunsaturated fatty acids, carotenoids, and antioxidant compounds (Fakhri et al., 2026; Patel et al., 2022). Among these metabolites, astaxanthin has attracted considerable commercial and scientific interest because of its strong antioxidant capacity and broad applications in aquaculture, nutraceuticals, cosmetics, and functional foods (Shah et al., 2016). Although *Haematococcus pluvialis* remains the most established natural source of astaxanthin, alternative microalgal platforms are being explored to improve growth performance, metabolic flexibility, and co-production potential (Debnath et al., 2024). *Chromochloris*

zofingiensis is particularly promising because it can accumulate both lipids and astaxanthin, making it a valuable system for the integrated production of energy-dense lipids and high-value antioxidant carotenoids (Zhang et al., 2021).

The accumulation of astaxanthin in green microalgae is closely associated with cellular stress responses (Xing et al., 2025). Under unfavorable conditions, such as nutrient limitation, high light, salinity, or oxidative pressure, microalgal cells often redirect carbon flux from growth-related metabolism toward storage lipids and secondary carotenoids (Fakhri et al., 2025; Gorgich et al., 2021; Xing et al., 2025). In *C. zofingiensis*, this metabolic flexibility is particularly important because lipid droplets may serve as deposition sites for secondary carotenoids, thereby enabling the coordinated accumulation of neutral lipids and astaxanthin (Mao et al., 2020). However, conventional stress-based induction often involves a productivity trade-off. Severe stress may enhance target metabolite accumulation, but it can also reduce cell growth, chlorophyll content, photosynthetic activity, and final biomass productivity (Kou et al., 2020). Therefore, a central challenge in microalgal biotechnology is to identify stressors that can activate protective and secondary metabolism without causing excessive physiological damage.

Nanoparticles have emerged as potential modulators of microalgal metabolism due to their large surface area, high surface reactivity, and ability to interact with cellular surfaces (Fazelian and Yousefzadi, 2020). Zinc oxide nanoparticles (ZnO-NPs) are of particular interest because zinc is an essential micronutrient involved in many enzymatic and photosynthetic processes. At the same time, ZnO-NPs can act as abiotic stressors through Zn^{2+} release, reactive oxygen species (ROS) generation, and direct nanoparticle–cell interactions (Khalafi et al., 2019; Moezzi et al., 2012). Thus, ZnO-NPs can be interpreted not only as toxicants but also as concentration-dependent nano-stressors whose biological effects may range from metabolic stimulation to cytotoxicity.

The toxicity of ZnO-NPs to microalgae has been widely documented. ZnO-NPs can attach to algal cell surfaces, reduce light availability, damage membranes, disrupt chloroplast structure, promote oxidative stress, and inhibit growth (Yung et al., 2017; Zakharova et al., 2025). In *Chlorella vulgaris*, exposure to ZnO-NP reduced cell viability and induced oxidative damage, as indicated by increased lipid peroxidation and altered antioxidant responses (Suman et al., 2015). In *Spirulina platensis*, ZnO-NPs caused concentration- and time-dependent reductions in biomass, chlorophyll, carotenoids, and phycocyanin, accompanied by severe cellular damage (Djearamane et al., 2018). Similar cytotoxic effects, including zinc accumulation, biomass reduction, pigment loss, and morphological injury, have been reported in *H. pluvialis* exposed to increasing concentrations of ZnO-NP (Djearamane et al., 2019). These findings indicate that concentration, exposure duration, algal species, particle behavior, medium composition, aggregation, and dissolution dynamics strongly influence ZnO-NP toxicity.

Nevertheless, the same mechanisms associated with toxicity may also trigger adaptive metabolism when exposure remains below the lethal threshold. This biphasic response is consistent with hormesis, in which low-to-moderate stress activates cellular defense pathways, whereas excessive stress suppresses physiological performance. For example, Kaliamurthi et al. (2019) reported that ZnO-NPs enhanced oxygen evolution, carotenoids, protein, starch, neutral lipids, and triacylglycerol in *Chlorella* sp. at an appropriate concentration. Similarly, Nasri et al. (2021) showed that ZnO-NPs increased astaxanthin production in *H. pluvialis*, but concentrations above the optimal range became toxic and reduced microalgal viability. The aforementioned studies demonstrate that ZnO-NPs can exert nanobiostimulant effects only when applied within a restricted sublethal concentration range.

Despite these advances, most previous studies have examined ZnO-NPs primarily from an ecotoxicological perspective, focusing on growth inhibition, oxidative damage, pigment degradation, and cell damage (Djearamane et al., 2019; Suman et al., 2015; Yung et al., 2017). Limited information is available on whether controlled exposure to ZnO NPs can redirect metabolism in *C. zofingiensis*, a species that produce both lipids and astaxanthin. This gap is important because the boundary between toxicity and biostimulation may determine whether ZnO-NPs suppress cellular function or enhance the accumulation of target metabolites.

Therefore, this study aimed to evaluate the concentration-dependent effects of ZnO-NPs on growth, biomass production, photosynthetic pigments, astaxanthin accumulation, protein content, and lipid content in *C. zofingiensis*. We hypothesized that low-to-moderate ZnO-NP exposure induces adaptive metabolic reprogramming,

whereas excessive exposure suppresses pigment accumulation and biochemical productivity. The novelty of this study lies in defining the physiological boundary between ZnO-NP toxicity and nano-biostimulation in *C. zofingiensis*, providing a basis for optimizing nanoparticle-assisted production of high-value microalgal metabolites.

MATERIALS AND METHODS

Strain and cultivation medium

C. zofingiensis UTEX 32 was obtained from the University of Texas Culture Collection of Algae. The strain was cultivated in sterilized BG-11 medium prepared with distilled water. Prior to the experiment, the inoculum was acclimatized for five days under static culture conditions and subsequently maintained with continuous aeration. All cultures were incubated at 25 °C under a light intensity of 12,000 lux.

Zinc oxide nanoparticles

Commercial zinc oxide nanoparticles (ZnO-NPs) were obtained from the manufacturer [CV. Inovasi Teknologi Nano, Indonesia] and used as the zinc source in the nanoparticle treatments. According to the manufacturer's specification, the ZnO-NPs had a reported primary particle size of 57 nm, purity of ≥99%, and were supplied in powder form. Before use, the nanoparticles were stored in a sealed container at room temperature under dry conditions to minimize moisture absorption and particle aggregation. The ZnO-NPs were used as received without surface coating or chemical modification. Before biological application, the dry powder was visually inspected and handled under dry conditions to reduce moisture-induced clumping.

Experimental culture conditions

The experiment was arranged using a completely randomized design to evaluate the effects of zinc oxide nanoparticles (ZnO-NPs) on the growth and biochemical composition of *C. zofingiensis*. Six treatments were applied: a standard BG-11 control containing zinc sulfate heptahydrate (0.22 mg L^{-1}), zinc-free BG-11 medium without ZnO-NPs, and zinc-free BG-11 medium supplemented with ZnO-NPs at concentrations of 0.06, 6, 30, and 60 mg L^{-1}. Each treatment was performed in triplicate (n = 3). Cultures were grown in 500 mL bottle containing 400 mL working volume of culture medium. The selected exposure range was designed to represent zinc-free conditions, low-dose nanoparticle exposure (0.06 mg L^{-1}), moderate exposure (6 mg L^{-1}), and high-stress/toxicological exposure levels (30–60 mg L^{-1}). This wide concentration gradient was used to identify the physiological boundary between possible nano-biostimulation and ZnO-NP-induced inhibition in *C. zofingiensis*.

Prior to application, ZnO-NPs were dispersed in sterile distilled water and sonicated for 30 min to obtain a homogeneous suspension. All cultures were inoculated at an initial optical density of $OD_{680} = 0.12$ to ensure comparable starting biomass among treatments. The cultures were maintained for 9 days at 25 °C under 12,000 lux illumination with a 24:0 h light:dark photoperiod and continuous aeration without external CO_2 enrichment. The initial pH of the culture medium was 7, but it was not actively controlled during the experiment. Growth was monitored daily by collecting culture samples at 24 h intervals. At the end of cultivation, algal cells were harvested by centrifugation and dried at 55 °C until a constant weight was reached. The dried biomass was stored at −20 °C for subsequent analyses of protein, lipid, and astaxanthin.

Characterization of zinc oxide nanoparticles

The morphology and particle size distribution of ZnO-NPs were examined using scanning electron microscopy (SEM; FEI Inspect-21). Elemental composition was determined using energy-dispersive X-ray spectroscopy coupled with SEM (SEM-EDX; FEI Inspect-21). The crystalline structure of the nanoparticles was confirmed by X-ray diffraction analysis (XRD; PANalytical X'Pert Pro). These analyses were conducted to verify the morphology, elemental purity, and crystalline phase of the ZnO-NPs prior to biological application. For biological experiments, ZnO-NPs were dispersed in sterile distilled water by sonication for 30 min to obtain a working suspension before addition to the culture medium. Dispersion stability in BG-11 medium, hydrodynamic particle size distribution, zeta potential, and Zn^{2+} dissolution were not directly quantified in this study; therefore, the biological responses are interpreted as the integrated outcome of dry-particle properties, possible aggregation in the medium, nanoparticle–cell contact, and potential ionic Zn release.

Growth analysis

To evaluate the growth of *C. zofingiensis*, optical density at 680 nm (OD_{680}) was measured at 24-hour intervals using a UV–Vis spectrophotometer (GENESYS™, Thermo Scientific, USA). The OD_{680} values were used as an indirect indicator of cell density to monitor growth dynamics during cultivation.

Specific growth rate (m, d^{-1}) was calculated from OD_{680} values during the exponential growth period using the equation:

$$\mu\ (d^{-1}) = \frac{[Ln(Nt) - Ln(N0)]}{\Delta t} \quad (1)$$

where: OD_1 and OD_2 represent optical density at the beginning and the highest OD during the cultivation period, respectively, and t is cultivation time in days.

Biomass determination

Dry biomass was determined at the end of cultivation using a gravimetric filtration method. GF/C Whatman filter papers with a diameter of 47 mm were dried at 105 °C for 2 h, cooled in a desiccator for 30 min, and weighed to obtain the initial filter weight. A 10 mL culture sample was filtered through the pre-weighed filter paper using a vacuum filtration system and rinsed with 10 mL distilled water to remove residual salts. The filter paper containing algal biomass was dried again at 105 °C for 2 h, cooled in a desiccator, and weighed to obtain the final weight. Dry biomass was calculated as described by Fakhri et al. (2021).

Pigment analysis

Photosynthetic pigment analysis was performed using 2 mL of *C. zofingiensis* culture. The sample was centrifuged at 4.000 rpm for 15 min, and 1.8 mL of the supernatant was discarded. Absolute methanol (1.8 mL) was then added to the pellet for pigment extraction. The tube was wrapped in aluminum foil to prevent light-induced pigment degradation, vortexed thoroughly, sonicated for 5 min, and incubated in a water bath at 70 °C for 10 min. After extraction, the sample was vortexed again and centrifuged at 4000 rpm for 15 min.

The absorbance of the supernatant was measured at 480, 652, and 665 nm using a UV–Vis spectrophotometer. Chlorophyll a and chlorophyll b concentrations were calculated according to Ritchie (2006) and Fakhri et al. (2021), while total carotenoid content was determined according to Kim et al. (2012). The pigment concentrations were calculated using the following equations:

$$\text{Chl } a\ (\mu g\ mL^{-1}) = 16.5169 \times \times A_{665} - 8.0962 \times A_{652} \quad (2)$$

$$\text{Chl } b\ (\mu g\ mL^{-1}) = 27.4405 \times \times A_{652} - 12.1688 \times A_{665} \quad (3)$$

$$\text{Car}(\mu g\ mL^{-1}) = 4 \times A_{480} \quad (4)$$

Astaxanthin determination

Astaxanthin content was determined using a spectrophotometric method modified from Boussiba and Vonshak (1991). Briefly, 10 mL of algal culture was collected and centrifuged at 1800 × g for 15 min. The obtained cell pellet was washed with 5 mL of distilled water to eliminate residual culture medium. Chlorophyll was removed by resuspending the pellet in 5 mL of 5% (w/v) potassium hydroxide (KOH) prepared in 30% (v/v) methanol. The suspension was vortexed for 30 s and incubated in a water bath at 75 °C for 10 min. The sample was then centrifuged again at 1800 × g for 15 min, and the supernatant was discarded. When the supernatant remained green, indicating residual chlorophyll, the dechlorophyllation step was repeated until the supernatant became colorless.

The dechlorophyllated pellet was subsequently mixed with 25 µL of acetic acid and 5 mL of dimethyl sulfoxide (DMSO) to extract astaxanthin. The mixture was vortexed thoroughly, sonicated in an ultrasonic cleaner for 15 min, and incubated again at 75 °C for 10 min to improve pigment release. After centrifugation, the supernatant containing astaxanthin was collected, and its absorbance was measured at 530 nm using a spectrophotometer. The astaxanthin concentration, expressed in mg L^{-1}, and cellular astaxanthin content, expressed in mg g^{-1}, were calculated using the following equation (Li et al., 2012) using the following equation:

$$\textit{Astaxanthin concentration}\ (\text{mg } L^{-1}) = = \frac{A_{530} - 0.0107}{0.1556} \quad (5)$$

$$\textit{Cellular astaxanthin content}\ (\text{mg } g^{-1}) = = \frac{\textit{Astaxanthin concentration}}{\textit{Biomass concentration}} \quad (6)$$

Protein determination

Protein content was quantified using the Lowry assay, with bovine serum albumin (BSA) used as the calibration standard (Lowry et al., 1951). A BSA standard curve ranging from 0 to 1.000 μg mL^{-1} was established based on absorbance at 750 nm, showing strong linearity (R^2 = 0.99). The protein content of the samples was then calculated and expressed as a percentage of dry weight (DW).

Lipid analysis

Total lipid content was determined using a modified Bligh and Dyer extraction method (Bligh and Dyer, 1959), with nitrogen gas used during solvent evaporation. Pre-dried extraction vials were weighed to obtain the initial weight (A). Dried *C. zofingiensis* biomass was ground into fine powder, and 0.03 g of biomass was transferred into a centrifuge tube (B). A methanol–chloroform mixture (1:2, v/v; 3 mL) was added, and the sample was vortexed for 30 s at 3.000 rpm. Subsequently, 0.8 mL NaCl solution was added to facilitate phase separation.

After vortexing, the mixture formed three layers: an upper aqueous phase, a middle debris layer, and a lower lipid-containing chloroform phase. The sample was centrifuged at 2500 rpm for 2 min. The upper aqueous phase was removed, and the lower lipid phase was carefully collected into a pre-weighed vial. The extraction was repeated using the remaining debris to maximize lipid recovery. The combined lipid extract was evaporated under nitrogen gas, dried at 65 °C for 2 h, cooled in a desiccator, and weighed (C). Lipid content was calculated according to Amalia et al. (2026) and was expressed as % of dry weight (% DW), while lipid productivity was determined as mg L^{-1} d^{-1}:

$$Lipid\ content\ (\%\ DW) = \frac{C\text{-}A}{B} \times\ 100\% \quad (7)$$

where: A denotes the weight of the empty vial, B represents the dry biomass weight, and C indicates the weight of the vial after lipid extraction.

$$Lipid\ productivity\ (\text{mg}\ L^{-1}\ d^{-1}) = = \frac{W2\text{-}W1}{\Delta t} \times\ lipid\ content \quad (8)$$

where: $W1$ represents the biomass at the start of cultivation, while $W2$ represents the biomass harvested at the end of the cultivation period.

Statistical analysis

Data are presented as mean ± standard deviation based on the available biological replicates for each parameter. Normality and homogeneity of variance were assessed using the Shapiro–Wilk test and Levene's test, respectively. Data were analyzed using one-way ANOVA followed by Duncan's post hoc test at $p < 0.05$. For biochemical parameters measured using two biological replicates per treatment (n = 2), statistical comparisons were interpreted cautiously.

RESULTS AND DISCUSSION

Characteristics of ZnO nanoparticles

The physicochemical characterization of the commercial ZnO-NPs was conducted to verify particle morphology, elemental composition, and crystalline phase prior to biological application. SEM analysis revealed that the commercial ZnO-NPs exhibited irregular quasi-spherical particles with dense agglomeration and heterogeneous distribution (Figure 1). The estimated primary particle size was approximately 50–100 nm, while larger secondary aggregates were observed. This phenomenon is typical for ZnO-NPs because their high surface energy and large surface-to-volume ratio promote interparticle attraction and agglomeration (Moezzi et al., 2012; Yung et al., 2017). Similar agglomerated ZnO-NPs with particle sizes of 39.7–49.6 nm and 46.7–56.4 nm have been reported in *S. platensis* (Djearamane et al., 2018) and *H. pluvialis* (Djearamane et al., 2019).

The EDX spectrum confirmed the presence of Zn and O without detectable impurity peaks, supporting the high elemental purity of the commercial ZnO-NPs. The atomic composition showed O at 56.87% and Zn at 43.13%, indicating an oxygen-rich ZnO surface. Such surface oxygen species may contribute to defect-related reactivity and potential biological activity (Ma et al., 2013). The XRD pattern showed sharp diffraction peaks corresponding to the hexagonal wurtzite phase of ZnO, consistent with reported diffraction profiles of ZnO-NPs (Moezzi et al., 2012). Overall, SEM–EDX–XRD

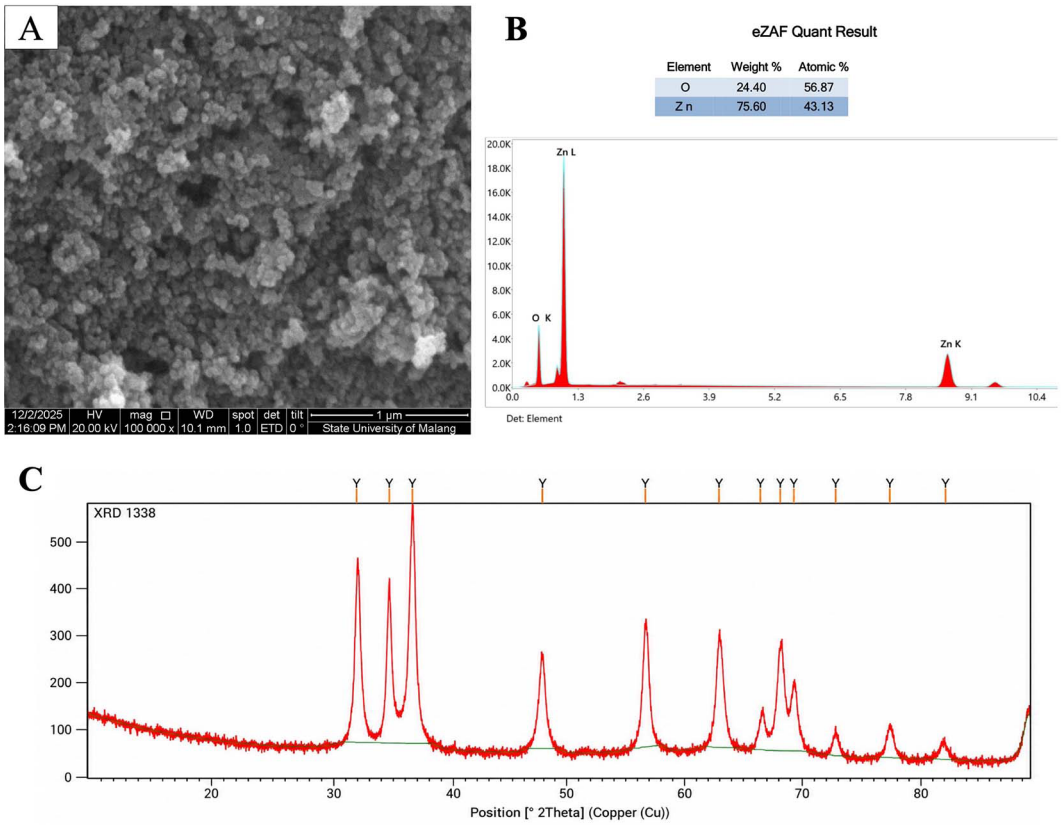

Figure 1. Physicochemical characterization of synthesized ZnO nanoparticles (ZnO-NPs).
(A) SEM micrograph showing agglomerated ZnO-NPs with irregular quasi-spherical morphology.
(B) EDX spectrum confirming Zn and O as the major elemental constituents.
(C) XRD pattern indicating the crystalline hexagonal wurtzite structure of ZnO-NPs

analyses confirmed that the commercial ZnO-NPs consisted of crystalline, phase-pure ZnO-NPs, where nanosized primary particles were assembled into larger agglomerates. Because nanoparticle behavior in aqueous culture can differ from dry-particle characteristics, the present SEM-EDX-XRD results should be interpreted together with possible aggregation, particle-cell contact, and Zn^{2+} release in BG-11 medium.

Growth and biomass *C. zofingiensis*

The growth curve showed that *C. zofingiensis* increased progressively in all treatments, but the response was concentration-dependent (Figure 2). The control and 0 mg L^{-1} groups showed the highest optical density, reaching approximately OD_{680} 1.25–1.36 by day 8–9. A low ZnO-NP dose (0.06 mg L^{-1}) initially supported growth during the early phase, but the culture declined after day 6, suggesting delayed stress. At 6 mg L^{-1}, growth remained relatively stable and reached a final OD close to the control, whereas higher concentrations, particularly 30 and 60 mg L^{-1}, suppressed OD accumulation from the mid-exponential phase onward. This pattern was supported by the biomass data (Figure 2), where the control produced the highest biomass (0.85±0.058 g L^{-1}), followed by 0 and 6 mg L^{-1} (0.79 g L^{-1}), while 0.06, 30, and 60 mg L^{-1} showed lower final biomass (0.71–0.74 g L^{-1}).

Specific growth rate (SGR) and doubling time provided clear kinetic indications of concentration-dependent effects of ZnO-NPs on *C. zofingiensis* (Table 1). The highest SGR occurred in the zinc-free treatment (0 mg L^{-1}; 0.356 ± 0.005 d^{-1}) and standard BG-11 control (0.355 ± 0.036 d^{-1}), with the shortest doubling times of 1.929 ± 0.026 and 1.961 ± 0.199 d, respectively. At 0.06 mg L^{-1}, SGR decreased slightly to 0.345 ± 0.012 d^{-1}, while doubling time increased to 2.008 ± 0.067 d, indicating very low ZnO-NP exposure did not impair cell division. Higher concentrations reduced SGR to 0.320 ± 0.032, 0.290 ± 0.040, and 0.297 ± 0.003 d^{-1} at 6, 30, and 60 mg L^{-1}, respectively, with longer doubling times of 2.174

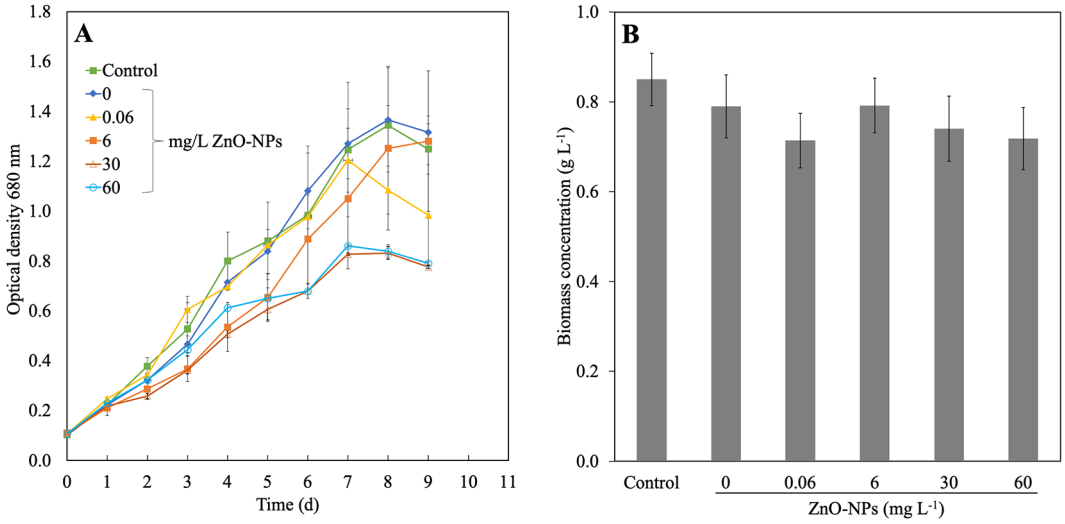

Figure 2. Effect of ZnO-NPs on the growth performance of C. zofingiensis. (A) Growth profile based on optical density at 680 nm during 9 days of cultivation under different ZnO-NP concentrations. (B) Final biomass concentration after ZnO-NP exposure. Values are presented as mean ± SD

± 0.219, 2.416 ± 0.331, and 2.337 ± 0.020 d. This reciprocal pattern confirms delayed proliferation under stronger nanoparticle pressure. Although 6 mg L^{-1} maintained a final OD close to the control, its lower SGR indicates stress. Overall, ZnO-NPs acted as concentration-dependent nano-stressors, likely through cell-surface attachment, membrane disturbance, Zn^{2+} release, and ROS formation.

These results are consistent with the dose-dependent effects of ZnO-NPs reported in microalgae. Kaliamurthi et al. (2019) found that 50 mg L^{-1} ZnO-NPs enhanced Chlorella growth, whereas higher doses did not completely inhibit growth but imposed stronger physiological stress. In contrast, Aravantinou et al. (2017) showed that ZnO-NP toxicity in *Scenedesmus rubescens* depended strongly on concentration, exposure time, and culture medium, with higher levels markedly suppressing algal growth. Similarly, Djearamane et al. (2019) reported dose- and time-dependent zinc accumulation, biomass loss, and pigment reduction in *H. pluvialis* exposed to ZnO-NPs.

Mechanistically, the observed inhibition at 30–60 mg L^{-1} may result from combined nanoparticle-specific and ionic effects. ZnO-NPs can attach to the algal surface, reduce light penetration through shading, disturb cell membrane integrity, and release Zn^{2+}, which may trigger reactive oxygen species formation and oxidative stress (Ma et al., 2013; Suman et al., 2015). At moderate levels, however, Zn may still act as an essential micronutrient involved in carbonic anhydrase activity, photosynthetic carbon acquisition, and antioxidant regulation.

Table 1. Specific growth rate and doubling time of Chromochloris zofingiensis exposed to different concentrations of ZnO-NPs

ZnO-NPs treatment (mg L^{-1})	SGR (d^{-1})	Doubling time (d)
Control	0.355±0.036	1.961±0.199
0	0.356±0.005	1.929±0.026
0.06	0.345±0.012	2.008±0.067
6	0.320±0.032	2.174±0.219
30	0.290±0.040	2.416±0.331
60	0.297±0.003	2.337±0.020

Note: Values are presented as mean ± standard deviation. The control treatment refers to standard BG-11 medium containing $ZnSO_4 \cdot 7H_2O$, while the 0 mg L^{-1} treatment refers to zinc-free BG-11 medium without ZnO-NPs.

Effect of ZnO-NPs on chlorophyll a+b, carotenoid, and astaxanthin synthesis

Figures 3 and 4 show that ZnO-NPs altered pigment metabolism in *C. zofingiensis* in a concentration-dependent manner. Chlorophyll *a*+*b* was significantly higher in the control, 0 mg L^{-1}, and 0.06 mg L^{-1} treatments than in 6 mg L^{-1} and other treatments ($p < 0.05$), indicating that photosynthetic pigment accumulation was maintained under zinc-free conditions and very low ZnO-NP exposure. In contrast, chlorophyll *a*+*b* declined sharply at 6, 30, and 60 mg L^{-1}, showing that moderate-to-high exposure impaired the

photosynthetic pigment system. Figure 3C further confirmed that chlorophyll reduction increased with ZnO-NP concentration, reaching approximately 60–70% relative to the control. Chlorophyll was therefore the most sensitive pigment fraction under ZnO-NP stress. This sensitivity may reflect disruption of chloroplast ultrastructure, inhibition of pigment biosynthesis, and interference with pigment-protein complexes involved in light harvesting (Wang et al., 2016). Reduced expression of chlorophyll biosynthesis genes and photosystem I structural proteins under ZnO-NP exposure has also been reported, suggesting that pigment loss can coincide with chloroplast and membrane damage (Azarin et al., 2023).

Total carotenoids followed a similar but less severe pattern. Carotenoid content decreased under 6, 30, and 60 mg L^{-1} ZnO-NPs, but the reduction was smaller than that observed for chlorophyll *a+b*. Figure 3D confirmed a gradual increase in carotenoid reduction with increasing ZnO-NP concentration, from negligible reduction at 0 mg L^{-1} to approximately 33–45% at 6–60 mg L^{-1}. The weaker decline in carotenoids suggests that *C. zofingiensis* retained part of its antioxidant pigment pool under nanoparticle stress. This response is physiologically relevant because carotenoids serve as accessory pigments and nonenzymatic antioxidants that quench reactive oxygen species and dissipate excess excitation energy (Masojídek et al., 2013).

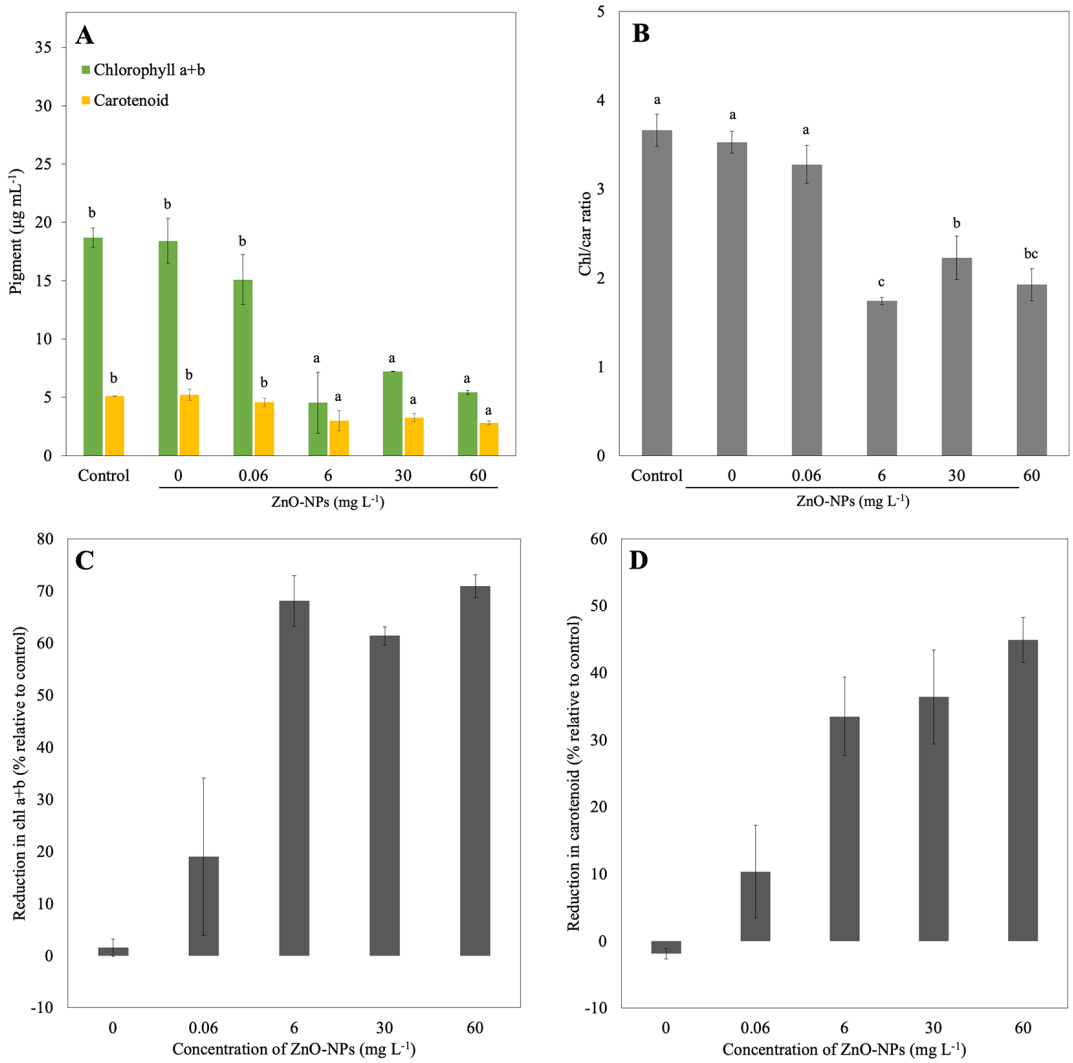

Figure 3. Effects of ZnO-NPs on photosynthetic pigment responses in Chromochloris zofingiensis. (A) Chlorophyll a+b and total carotenoid concentrations, (B) chlorophyll/carotenoid ratio, (C) percentage reduction in chlorophyll a+b relative to the control, and (D) percentage reduction in carotenoids relative to the control after exposure to different ZnO-NP concentrations. Values are presented as mean ± standard deviation. Different lowercase letters indicate significant differences among treatments based on Duncan's post hoc test ($p < 0.05$)

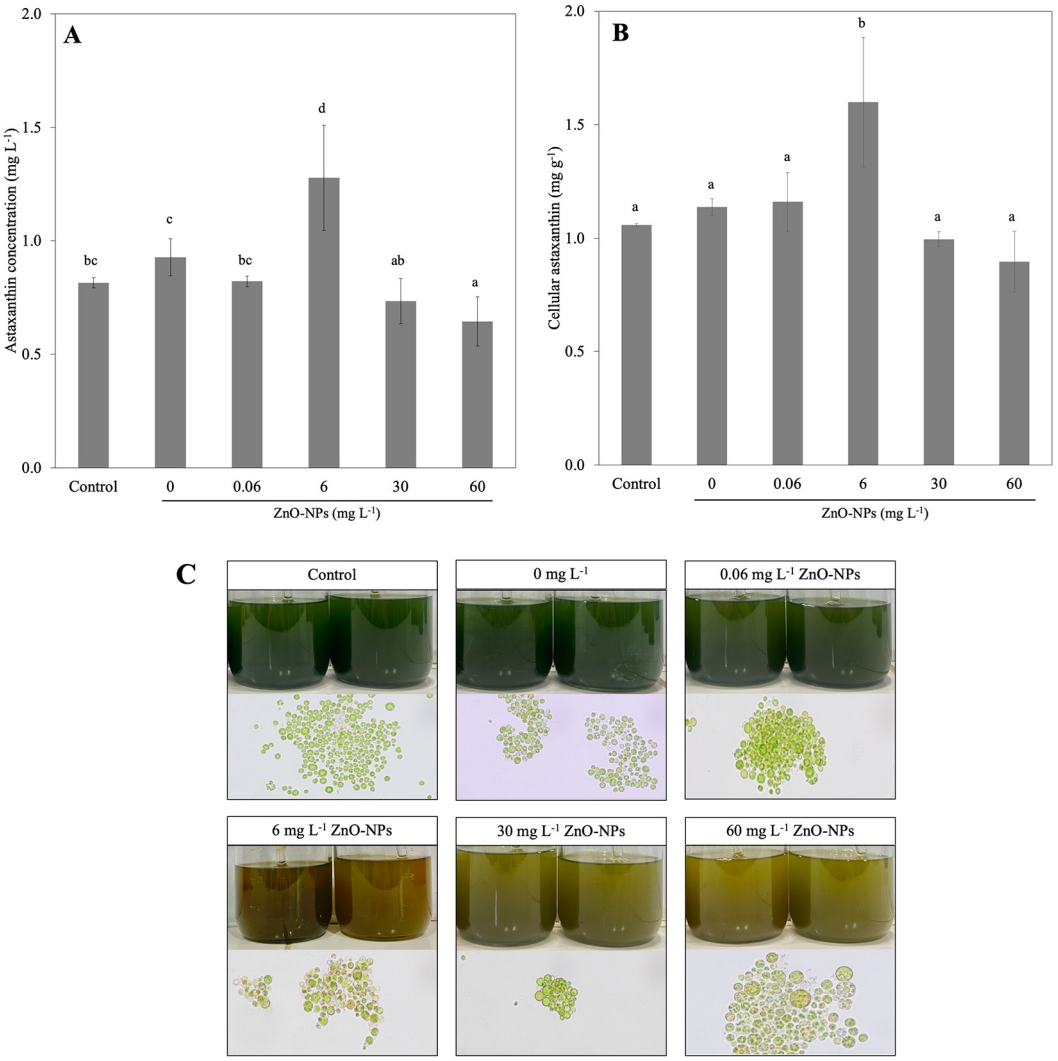

Figure 4. Effects of ZnO-NPs on astaxanthin accumulation and cell appearance in Chromochloris zofingiensis. (A) Astaxanthin concentration, (B) cellular astaxanthin content, and (C) visual and microscopic appearance of C. zofingiensis cultures after exposure to different ZnO-NP concentrations.
Values are presented as mean ± standard deviation. Different lowercase letters indicate significant differences among treatments based on Duncan's post hoc test ($p < 0.05$)

The chlorophyll/carotenoid ratio provided additional evidence of pigment reorganization. The ratio was highest in the control, 0 mg L^{-1}, and 0.06 mg L^{-1} treatments, indicating chlorophyll-dominated photosynthetic metabolism under non-stress or low-stress conditions. In contrast, the ratio declined significantly at 6, 30, and 60 mg L^{-1}, with the lowest value at 6 mg L^{-1}. This shift indicates selective chlorophyll suppression with comparatively greater carotenoid retention, reflecting a transition from photosynthetic activity toward stress defense.

Astaxanthin responded differently from chlorophyll and total carotenoids. The astaxanthin concentration was significantly highest ($p < 0.05$) at 6 mg L^{-1} ZnO-NPs, reaching approximately 1.28 mg L^{-1} (Figure 4A). Cellular astaxanthin content showed the same trend, with the 6 mg L^{-1} treatment producing a significantly higher value ($p < 0.05$) than all other treatments (Figure 4B). In contrast, astaxanthin concentration decreased at 30 and 60 mg L^{-1}, with the 60 mg L^{-1} treatment showing the significantly lowest value ($p < 0.05$). These findings indicate that 6 mg L^{-1} ZnO-NPs acted as an effective sublethal stress level for secondary carotenoid induction in C. zofingiensis. The significant increase in both volumetric astaxanthin concentration and cellular astaxanthin content suggests that astaxanthin enhancement resulted from increased intracellular accumulation rather than biomass variation alone. However, the decline at higher ZnO-NP

concentrations indicates that excessive exposure surpassed the adaptive threshold and impaired astaxanthin biosynthesis.

Visual observations supported the quantitative pigment data (Figure 4C). The control, 0 mg L^{-1}, and 0.06 mg L^{-1} cultures remained darker green, consistent with higher chlorophyll levels. Cultures exposed to 6, 30, and 60 mg L^{-1} shifted toward yellowish-green or brownish-green coloration, indicating chlorophyll degradation and altered pigment composition. Microscopy also showed paler and more clustered cells under higher ZnO-NP exposure, suggesting effects on cell condition and culture appearance through nanoparticle attachment, shading, pigment degradation, or physiological stress.

The simultaneous decline in chlorophyll *a*+*b* and increase in astaxanthin at 6 mg L^{-1} suggests a shift from growth-associated photosynthesis toward stress-defense metabolism. This response is consistent with hormesis, where moderate stress activates adaptive pathways but excessive stress suppresses physiological performance. Li et al. (2008) described astaxanthin biosynthesis as a protective mechanism against oxidative stress in green microalgae. Astaxanthin protects microalgae from photooxidative damage by quenching reactive oxygen species, stabilizing membranes, and reducing oxidative injury. Thus, astaxanthin enhancement at 6 mg L^{-1} indicates sufficient stress to activate defense metabolism without blocking secondary carotenoid biosynthesis.

Astaxanthin concentration and cellular content decreased at 30 and 60 mg L^{-1}, indicating that excessive ZnO-NP exposure exceeded the adaptive capacity of *C. zofingiensis*. Although moderate nanoparticle stress stimulated astaxanthin biosynthesis, higher concentrations likely caused physiological damage that reduced biosynthetic capacity and metabolic regulation. Nasri et al. (2021) reported a similar pattern in *H. pluvialis*, where ZnO-NPs enhanced astaxanthin production within an optimal range but reduced biomass and astaxanthin yield at excessive concentrations. The astaxanthin response therefore confirms a physiological boundary between nano-biostimulation and nanoparticle toxicity.

Effect of ZnO-NPs on protein and lipid content

ZnO-NPs changed the biochemical composition of *C. zofingiensis* in a concentration-dependent manner, particularly in relation to protein and lipid accumulation. Protein content ranged from approximately 8.6 to 21.7% DW across treatments (Figure 5A). The highest protein content was observed at 0.06 mg L^{-1} ZnO-NPs, reaching approximately 21.7% dry weight, followed by the 30 and 6 mg L^{-1} treatments. In contrast, the zinc-free treatment and the highest ZnO-NP concentration, 60 mg L^{-1}, showed lower protein accumulation. This pattern suggests that mild ZnO-NP exposure may support protein biosynthesis, whereas excessive exposure may suppress cellular metabolism. Lipid content showed a contrasting response (Figure 5B). The highest lipid contents were recorded in the zinc-free and 0.06 mg L^{-1} treatments, both reaching approximately 19% DW. The lowest lipid content was found at 6 mg L^{-1}, at around 12% DW. Although lipid content increased again at 30 and 60 mg L^{-1}, it remained lower than that observed in the zinc-free and 0.06 mg L^{-1} treatments.

Lipid productivity clarified the combined effect of lipid content and biomass formation (Figure 5C). Although the zinc-free and 0.06 mg L^{-1} treatments had high lipid content, their lipid productivity was lower than the control. Lipid productivity declined progressively from 6 to 60 mg L^{-1} ZnO-NPs, with the lowest value at 60 mg L^{-1}. This indicates that ZnO-NP stress reduced overall lipid output mainly by limiting biomass accumulation, even when lipid content was partly maintained.

These findings partly agree with previous reports, although the response appears to be highly species- and condition-dependent. Kaliamurthi et al. (2019) reported that ZnO-NPs enhanced protein, neutral lipid, and triacylglycerol accumulation in *Chlorella* sp., with 50 mg L^{-1} ZnO-NPs producing a strong increase in neutral lipid and triacylglycerol during short-term exposure. Aravantinou et al. (2017) also showed that ZnO-NPs could increase lipid content in *S. rubescens* under specific culture-medium conditions, particularly at low concentrations, and associated this response with oxidative stress-induced lipid accumulation. However, studies on *S. platensis* and *C. vulgaris* have shown that higher ZnO-NP exposure can reduce cell viability, damage membranes, and disrupt cellular metabolism, thereby limiting microalgae's capacity to maintain normal biochemical and pigment profiles.

The increase in protein content at 0.06 mg L^{-1} ZnO-NPs may reflect mild hormesis. At low concentrations, ZnO-NPs may release bioavailable

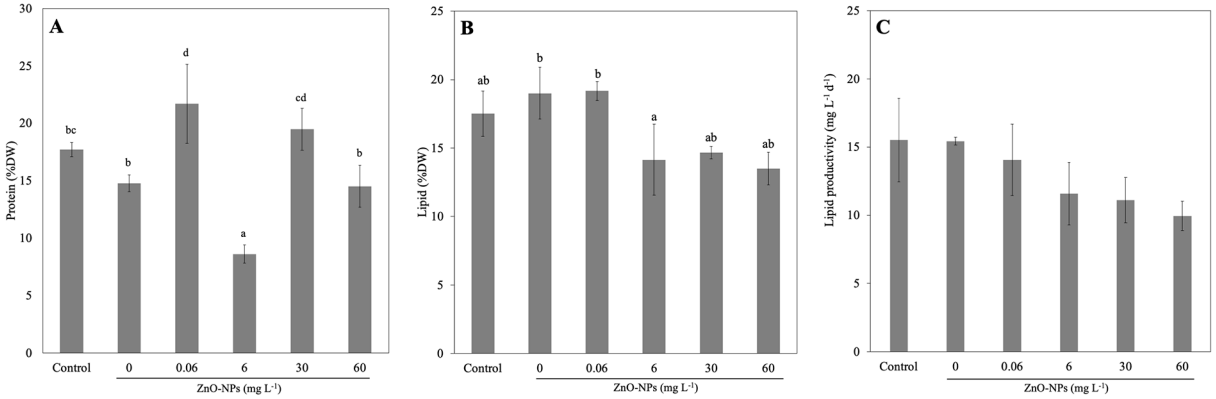

Figure 5. Effects of ZnO-NPs on biochemical composition and lipid productivity in Chromochloris zofingiensis. (A) Protein content, (B) lipid content, and (C) lipid productivity of C. zofingiensis after exposure to different ZnO-NP concentrations. Values are presented as mean ± standard deviation. Different lowercase letters indicate significant differences among treatments based on Duncan's post hoc test ($p < 0.05$)

Zn^{2+} at levels that support enzymatic activity without causing severe toxicity. Zinc is required by several proteins and enzymes, including carbonic anhydrase, alcohol dehydrogenase, and antioxidant-related proteins. Low ZnO-NP exposure may therefore enhance nitrogen assimilation, stress-response protein synthesis, and general metabolic activity. Conversely, reduced protein content at 60 mg L^{-1} suggests that ZnO-NP exposure exceeded cellular tolerance, impairing photosynthesis and protein biosynthesis through surface attachment, membrane disturbance, Zn^{2+} release, and ROS formation (Ma et al., 2013; Suman et al., 2015).

The lipid response should be interpreted together with pigment and astaxanthin data. At 6 mg L^{-1}, C. zofingiensis produced the highest astaxanthin concentration but the lowest lipid content, suggesting that carbon and reducing power were preferentially redirected toward secondary carotenoid biosynthesis rather than storage lipid accumulation. In green microalgae, astaxanthin biosynthesis is typically activated as part of antioxidant defense under oxidative stress, whereas lipid accumulation is more closely associated with nutrient limitation, carbon overflow, or prolonged stress. Thus, 6 mg L^{-1} ZnO-NPs may represent a threshold at which C. zofingiensis prioritizes astaxanthin formation over lipid storage. At 30–60 mg L^{-1}, partial lipid recovery may reflect stress-induced storage lipid formation, but the concurrent pigment reduction indicates that these concentrations exceeded the optimal adaptive range. Descriptively, the treatment-wise pattern suggested an inverse tendency between astaxanthin accumulation and lipid content, particularly at 6 mg L^{-1} ZnO-NPs, where astaxanthin reached its highest level while lipid content was lowest. Similarly, treatments maintaining higher chlorophyll *a*+*b* generally showed better biomass synthesis.

CONCLUSIONS

ZnO-NPs exerted a concentration-dependent dual effect on *C. zofingiensis*, ranging from adaptive nano-biostimulation to physiological inhibition. Moderate exposure, particularly 6 mg L^{-1}, enhanced astaxanthin accumulation and productivity despite reductions in chlorophyll a+b and lipid content, indicating a metabolic trade-off among photosynthetic pigment maintenance, storage lipid accumulation, and secondary carotenoid biosynthesis. Higher concentrations exceeded cellular adaptive capacity, causing stronger pigment suppression and reduced biochemical performance. This study identifies the physiological boundary between ZnO-NP-induced toxicity and nano-biostimulation in C. zofingiensis and shows that carefully controlled nanoparticle stress can redirect metabolism toward high-value carotenoid accumulation. However, the findings should be interpreted in light of unmeasured aggregation behavior, hydrodynamic size, zeta potential, and Zn^{2+} dissolution in the culture medium. Future work should quantify oxidative stress markers, zinc uptake and speciation, nanoparticle stability in BG-11 medium, gene expression related to

carotenoid and lipid biosynthesis, and scale-up performance to validate the practical use of ZnO-NPs in microalgal biotechnology.

Acknowledgements

The authors sincerely thank the Faculty of Fisheries and Marine Science, Universitas Brawijaya, for providing the laboratory facilities required to conduct this study.

REFERENCES

1. Amalia, D. I. N., Supriatin, F. E., Mohammed, I. A., Arifin, N. B., Yuniarti, A., Fakhri, M. (2026). Moderate phosphate supply optimizes lipid productivity and pigment accumulation in the freshwater microalga *Monoraphidium braunii*. *Ecological Engineering & Environmental Technology*, *27*(5), 33–42.
2. Aravantinou, A. F., Andreou, F., Manariotis, I. D. (2017). Long-term toxicity of ZnO nanoparticles to *Scenedesmus rubescens* cultivated in different media. *Scientific Reports*, (May), 1–11. https://doi.org/10.1038/s41598-017-13517-7
3. Azarin, K., Usatov, A., Minkina, T., Duplii, N., Kasyanova, A., Fedorenko, A., Khachumov, V., Mandzhieva, S., Rajput, V. D. (2023). Effects of bulk and nano-ZnO particles on functioning of photosynthetic apparatus in barley (*Hordeum vulgare* L.). *Environmental Research*, *216*, 114748. https://doi.org/https://doi.org/10.1016/j.envres.2022.114748
4. Bligh, E.G. and Dyer, W. J. (1959). A rapid method of total lipid extraction and purification. *Canadian Journal of Biochemistry and Physiology*, *37*(8), 911–917.
5. Boussiba, S., Vonshak, A. (1991). Astaxanthin accumulation in the green alga *Haematococcus pluvialis*. *Plant Cell Physiol.*, *32*(7), 1077–1082.
6. Debnath, T., Bandyopadhyay, T. K., Vanitha, K., Bobby, M. N., Nath Tiwari, O., Bhunia, B., & Muthuraj, M. (2024). Astaxanthin from microalgae: A review on structure, biosynthesis, production strategies and application. *Food Research International*, *176*, 113841. https://doi.org/https://doi.org/10.1016/j.foodres.2023.113841
7. Djearamane, S., Lim, Y. M., Wong, L. S. (2018). Cytotoxic effects of zinc oxide nanoparticles on cyanobacterium *Spirulina* (*Arthrospira*) *platensis*. *PeerJ*, *6*, e4682. https://doi.org/10.7717/peerj.4682
8. Djearamane, S., Lim, Y. M., Wong, L. S. (2019). Cellular accumulation and cytotoxic effects of zinc oxide nanoparticles in microalga *Haematococcus pluvialis*. *PeerJ*, *7*, e7582. https://doi.org/10.7717/peerj.7582
9. Fakhri, M., Fauzan, M. R., Suprastyani, H., Dailami, M., Weerakkody, W. S., Arifin, N. B. (2026). Mixotrophic culture of *Monoraphidium braunii* using glucose on the increase of biomass, protein, and lipid productivity. *Journal of Ecological Engineering*, *27*(2), 169–177. https://doi.org/https://doi.org/10.12911/22998993/211162
10. Fakhri, M., Kristianti, E., Mahariawan, I. M. D., Buwono, N. R., Puspitasari, Y. E., Rahardjo, S. S. P., Kusuma, W. E., Arifin, N. B., Yuniarti, A., Hariati, A. M. (2025). High phosphorus concentration induces lipid accumulation in *Chlorella pyrenoidosa* under nitrogen deficiency. *Journal of Ecological Engineering*, *26*(5), 213–219. https://doi.org/10.12911/22998993/201202
11. Fakhri, M., Riyani, E., Ekawati, A. W., Arifin, N. B., Yuniarti, A., Widyawati, Y., Saputra, I. K., Samuel, P. D., Arif, M. Z., Hariati, A. M. (2021). Biomass, pigment production, and nutrient uptake of *Chlorella* sp. under different photoperiods. *Biodiversitas*, *22*(12), 5344–5349. https://doi.org/10.13057/biodiv/d221215
12. Fazelian, N., Yousefzadi, M. (2020). Algal response to metal oxide nanoparticles: Aanalysis of growth, protein content, and fatty acid composition. *BioEnergy Research*, *13*, 944–954. https://doi.org/10.1007/s12155-020-10099-7 Algal
13. Gorgich, M., Martins, A. A., Mata, T. M., Caetano, N. S. (2021). Composition, cultivation and potential applications of *Chlorella zofingiensis* – A comprehensive review. *Algal Research*, *60*(September). https://doi.org/10.1016/j.algal.2021.102508
14. Kaliamurthi, S., Selvaraj, G., Elibol, Z., Demir, A. (2019). The relationship between *Chlorella* sp. and zinc oxide nanoparticles: Changes in biochemical, oxygen evolution, and lipid production ability. *Process Biochemistry*, *85*, 43–50.
15. Khalafi, T., Buazar, F., Ghanemi, K. (2019). Phycosynthesis and Enhanced Photocatalytic Activity of zinc oxide nanoparticles toward organosulfur pollutants. *Scientific Reports*, *9*, 6866. https://doi.org/10.1038/s41598-019-43368-3
16. Kou, Y., Liu, M., Sun, P., Dong, Z., Liu, J. (2020). High light boosts salinity stress-induced biosynthesis of astaxanthin and lipids in the green alga *Chromochloris zofingiensis*. *Algal Research*, *50*, 101976. https://doi.org/https://doi.org/10.1016/j.algal.2020.101976
17. Li, Y., Miao, F., Geng, Y., Lu, D., Zhang, C., Zeng, M. (2012). Accurate quantification of astaxanthin from Haematococcus crude extract spectrophotometrically. *Chinese Journal of Oceanology and Limnology*, *30*(4), 627–637.
18. Li, Y., Sommerfeld, M., Chen, F., Hu, Q. (2008). Consumption of oxygen by astaxanthin biosynthesis: A protective mechanism against oxidative stress in

Haematococcus pluvialis (Chlorophyceae). *Journal of Plant Physiology*, *165*(17), 1783–1797. https://doi.org/https://doi.org/10.1016/j.jplph.2007.12.007

19. Lowry, O. H., Rosebrpugh, N. J., Farr, A. L., Randall, R. J. (1951). Protein measurement with the Folin phenol reagent. *The Journal of Biological Chemistry*, *193*(1), 265–275. https://doi.org/10.1016/s0021-9258(19)52451-6
20. Ma, H., Williams, P. L., Diamond, S. A. (2013). Ecotoxicity of manufactured ZnO nanoparticles – A review. *Environmental Pollution*, *172*, 76–85. https://doi.org/https://doi.org/10.1016/j.envpol.2012.08.011
21. Mao, X., Zhang, Y., Wang, X., Liu, J. (2020). Novel insights into salinity-induced lipogenesis and carotenogenesis in the oleaginous astaxanthin-producing alga *Chromochloris zofingiensis*: A multi-omics study. *Biotechnology for Biofuels*, *13*(1), 1–24. https://doi.org/10.1186/s13068-020-01714-y
22. Masojídek, J., Torzillo, G., Koblížek, M. (2013). Photosynthesis in Microalgae. In A. Richmond & H. Qiang (Eds.), *Handbook of Microalgal Culture: Applied Phycology and Biotechnology* (pp. 21–36). https://doi.org/https://doi.org/10.1002/9781118567166.ch2
23. Moezzi, A., McDonagh, A. M., Cortie, M. B. (2012). Zinc oxide particles: Synthesis, properties and applications. *Chemical Engineering Journal*, *185–186*, 1–22. https://doi.org/https://doi.org/10.1016/j.cej.2012.01.076
24. Nasri, N., Keyhanfar, M., Behbahani, M., Dini, G. (2021). Enhancement of astaxanthin production in *Haematococcus pluvialis* using zinc oxide nanoparticles. *Journal of Biotechnology*, *342*, 72–78. https://doi.org/10.1016/j.jbiotec.2021.10.004
25. Patel, A. K., Tambat, V. S., Chen, C.-W., Chauhan, A. S., Kumar, P., Vadrale, A. P., Huang, C.-Y., Dong, C.-D., Singhania, R. R. (2022). Recent advancements in astaxanthin production from microalgae: A review. *Bioresource Technology*, *364*, 128030. https://doi.org/https://doi.org/10.1016/j.biortech.2022.128030
26. Shah, M. M. R., Liang, Y., Cheng, J. J., Daroch, M. (2016). Astaxanthin-producing green microalga *Haematococcus pluvialis*: From single cell to high value commercial products. *Frontiers in Plant Science*, *7*, 531. https://doi.org/10.3389/fpls.2016.00531
27. Suman, T. Y., Rajasree, S. R. R., Kirubagaran, R. (2015). Evaluation of zinc oxide nanoparticles toxicity on marine algae *Chlorella vulgaris* through flow cytometric, cytotoxicity and oxidative stress analysis. *Ecotoxicology and Environmental Safety*, *113*, 23–30. https://doi.org/10.1016/j.ecoenv.2014.11.015
28. Wang, X., Yang, X., Chen, S., Li, Q., Wang, W., Hou, C., Gao, X., Wang, L., Wang, S. (2016). Zinc oxide nanoparticles affect biomass accumulation and photosynthesis in Arabidopsis. *Frontiers in Plant Science*, *7*, 559. https://doi.org/10.3389/fpls.2016.00559
29. Xing, H., Zhou, N., Liu, K., Yan, X., Li, W., Sun, X., Zhang, L., Liu, F., Xu, N., Hu, C. (2025). Nitrogen deprivation drives red motile cell formation in *Haematococcus pluvialis*: physiological and transcriptomic insights. *Metabolites*, *15*(6), 1–25. https://doi.org/10.3390/metabo15060388
30. Yung, M. M. N., Fougères, P., Leung, Y. H., Liu, F., Djuri, B., Giesy, J. P., Leung, K. M. Y. (2017). Physicochemical characteristics and toxicity of surface-modified zinc oxide nanoparticles to freshwater and marine microalgae. *Scientific Reports*, *7*, 15909. https://doi.org/10.1038/s41598-017-15988-0
31. Zakharova, O. V, Vasyukova, I. A., Chebotaryova, S. P., Koiava, E. Y., Razlivalova, S. S., Grigoriev, G. V, Baranchikov, P. A., Gusev, A. A. (2025). Dose-dependent effects of zno nanoparticles towards the microalgae Lobosphaera: Compensation of salt stress at low concentration and toxicity at high concentrations. *International Journal of Molecular Sciences*, *26*, 9455.
32. Zhang, Y., Ye, Y., Bai, F., Liu, J. (2021). The oleaginous astaxanthin - producing alga *Chromochloris zofingiensis*: potential from production to an emerging model for studying lipid metabolism and carotenogenesis. *Biotechnology for Biofuels*, *14*, 119. https://doi.org/10.1186/s13068-021-01969-z